Chapter 5
Two-Dimensional Calcium Release

The essence of calcium-induced calcium release is once more illustrated in Fig. 5.1. This figure is very similar to Fig. 2.1 on page 24 except that the box surrounded by a thin red line is now slightly extended. This is meant to illustrate that the model is now extended to account for changes in the calcium concentration of the junctional sarcoplasmic reticulum (JSR) space (see Fig. 5.1); so we now consider a two-dimensional (2D) model where the concentration of the dyad ($\bar{x} = \bar{x}(t)$) and the JSR ($\bar{y} = \bar{y}(t)$) vary, recalling that the bar notation indicates stochastic variables. The concentration of the cytosol and the network sarcoplasmic reticulum (NSR) are still kept constant and we still ignore L-type calcium currents. An illustration of the mathematical model under consideration is given in Fig. 5.2.

The basic steps of the analysis of the 2D problem follow the steps of the analysis of the one-dimensional (1D) problem. We will start our analysis of the 2D problem by formulating a 2×2 system of stochastic differential equations giving the dynamics of the calcium concentration of the dyad and of the JSR. This model will be used as a basis for Monte Carlo simulations. By following the steps above, we also derive a 2D deterministic equation describing the probability density functions of the open and closed states. A numerical method for this system will be presented and, again, we will find that it is reasonable to focus on steady state computations. The probability density model will be extended to account for open or closed state blockers and, as above, we will see that we can find very good closed state blockers for CO-mutations (see page 16).

A. Tveito, G.T. Lines, *Computing Characterizations of Drugs for Ion Channels and Receptors Using Markov Models*, Lecture Notes in Computational Science and Engineering 111, DOI 10.1007/978-3-319-30030-6_5

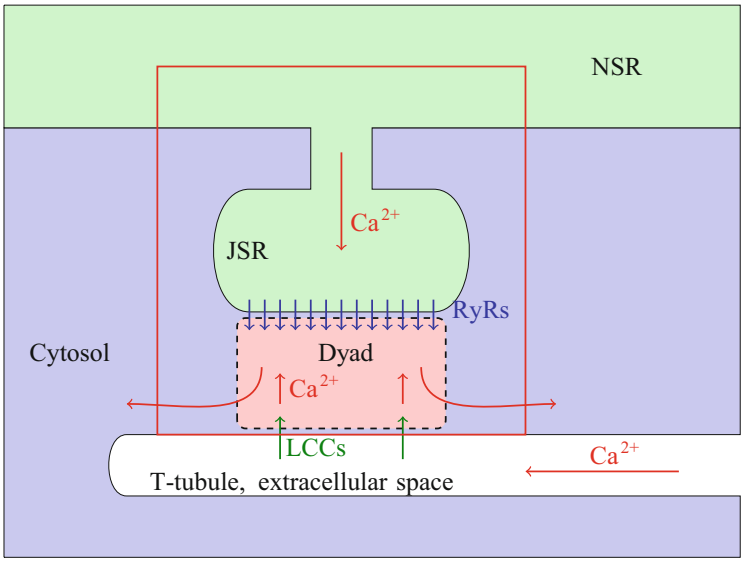

Fig. 5.1 As above, this figure illustrates the components involved in calcium-induced calcium release: the T-tubule, the dyad, the sarcoplasmic reticulum (SR) represented by the JSR and NSR and the cytosol. In this chapter, we concentrate on the dynamics in the box surrounded by a *thin red line*. We assume that the concentrations of the cytosol (c_0) and of the NSR (c_1) are constants and we ignore the LCCs. The variables of interest are the calcium concentrations of the dyad ($\bar{x} = \bar{x}(t)$) and the JSR ($\bar{y} = \bar{y}(t)$)

Cytosol, c_0	Dyad, $\bar{x}(t)$	JSR, $\bar{y}(t)$	NSR, c_1

Fig. 5.2 Sketch of a release unit. The cytosolic calcium concentration (c_0) and NSR calcium concentration (c_1) are assumed to be constant, while the concentrations of the dyad and JSR are given by $\bar{x} = \bar{x}(t)$ and $\bar{y} = \bar{y}(t)$, respectively. Note that $c_0 \ll c_1$

5.1 2D Calcium Release

The process of calcium release illustrated in Fig. 5.2 can be modeled as follows:

$$\bar{x}'(t) = \bar{\gamma}(t) v_r \, (\bar{y} - \bar{x}) + v_d \, (c_0 - \bar{x}) \,, \tag{5.1}$$

$$\bar{y}'(t) = \bar{\gamma}(t) v_r \, (\bar{x} - \bar{y}) + v_s \, (c_1 - \bar{y}) \,, \tag{5.2}$$

where v_r denotes the rate of release from the JSR to the dyad, v_d denotes the speed of calcium diffusion from the dyad to the cytosol, and v_s denotes the speed of calcium diffusion from the NSR to the JSR. Furthermore, $\bar{\gamma}(t)$ is a stochastic variable taking on two possible values, zero and one, with (as above) zero denoting a closed channel

and one denoting an open channel. The dynamics of $\bar{\gamma}$ are governed by the Markov model under consideration. Furthermore, we always assume that

$$c_1 \gg c_0 \text{ and } v_r, v_d, v_s > 0. \tag{5.3}$$

For the 2D case, we also assume[1] that

$$v_d v_s \geq v_r^2. \tag{5.4}$$

5.1.1 The 1D Case Revisited: Invariant Regions of Concentration

Suppose the speed of diffusion, v_s, from the JSR to the NSR becomes very large. From (5.2), we observe that the limiting case when $v_s \to \infty$ yields $y = c_1$ and thus the problem is in 1D and can be written

$$\bar{x}'(t) = \bar{\gamma}(t) v_r (c_1 - \bar{x}) + v_d (c_0 - \bar{x}),$$

which is exactly the problem we discussed in Chap. 2 (page 25). We analyzed this equation and saw that, when the channel is closed ($\gamma = 0$), the solution tends toward the equilibrium point represented by

$$x = c_0$$

and, when the channel is open, the equilibrium solution is given by

$$x = c_+ = (1 - \alpha) c_1 + \alpha c_0,$$

where

$$\alpha = \frac{v_d}{v_r + v_d}.$$

Based on this, we concluded that if the initial concentration is in the interval $[c_0, c_+]$, the solution will always remain in this interval. The reason for this is that if the channel is closed, the solution will decrease toward c_0 and, if the channel is open, the solution will increase toward c_+. For closed channels, c_0 is a stable equilibrium and, similarly, if the channel is open, c_+ is a stable equilibrium.

[1] This is a technical assumption needed in an argument below.

5.1.2 Stability of Linear Systems

Before we consider the 2D case, we need to recall some basic properties of linear systems of ordinary differential equations. For a system of the form

$$x'(t) = Ax,$$

where A is a matrix and the unknown x is a vector, we know that the equilibrium solution $x = 0$ is stable, provided that the real part of all the eigenvalues of A is negative. However, the systems under consideration here are of the form

$$x'(t) = Ax + b, \tag{5.5}$$

where b is a known vector. In the case of a non-singular matrix A, the equilibrium solution is given by

$$x^* = -A^{-1}b \tag{5.6}$$

and we are interested in the stability of this solution. To assess the stability, we define

$$e = x - x^*$$

and observe that

$$e'(t) = x'(t) = Ax + b = Ax - Ax^* = Ae$$

and, of course, $e = 0$ is a stable equilibrium of the system

$$e' = Ae,$$

provided that the real part of all the eigenvalues of A are negative. Therefore, the equilibrium solution (5.6) of the system (5.5) is stable under the same condition. With these observations at hand, we are ready to try to understand the dynamics of the system (5.1) and (5.2).

5.1.3 Convergence Toward Two Equilibrium Solutions

Our aim is now to understand the dynamics of the 2D case and we start by considering the system when the channel is closed.

5.1.3.1 Equilibrium Solution for Closed Channels

In this case, the system (5.1) and (5.2) is quite simple, since there is no communication between the dyad and the JSR. The system is

$$x'(t) = v_d\,(c_0 - x)\,, \tag{5.7}$$

$$y'(t) = v_s\,(c_1 - y)\,, \tag{5.8}$$

and the stable equilibrium solution of this system is given by

$$x_c = c_0,$$

$$y_c = c_1.$$

5.1.3.2 Equilibrium Solution for Open Channels

The more interesting case is when the channel is open. Then the system reads

$$x'(t) = v_r\,(y - x) + v_d\,(c_0 - x)\,, \tag{5.9}$$

$$y'(t) = v_r\,(x - y) + v_s\,(c_1 - y)\,, \tag{5.10}$$

and the equilibrium solution is given by

$$x_o = \alpha c_1 + (1 - \alpha)\,c_0,$$

$$y_o = \beta c_1 + (1 - \beta)\,c_0,$$

where

$$\alpha = \frac{v_r v_s}{v_d\,(v_r + v_s) + v_r v_s},$$

$$\beta = \frac{v_s\,(v_d + v_r)}{v_d\,(v_r + v_s) + v_r v_s}.$$

It is useful, but not surprising, to note that

$$y_o - x_o = (\beta - \alpha)\,(c_1 - c_0) = \frac{v_s v_d}{v_d\,(v_r + v_s) + v_r v_s}\,(c_1 - c_0) > 0,$$

since c_1 is assumed to be larger than c_0 (see (5.3)).

5.1.3.3 Stability of the Equilibrium Solution

Whether the equilibrium solution for open channels is stable remains to be seen. As noted above, this can be determined by invoking the eigenvalues of the system matrix, which, in this case, are given by

$$A = \begin{pmatrix} -(v_r + v_d) & v_r \\ v_r & -(v_r + v_s) \end{pmatrix}.$$

Since the matrix is symmetric, the eigenvalues are real, so it is sufficient to see if they are always non-positive. The eigenvalues are given by

$$\lambda_- = \frac{1}{2}\left(-\sqrt{(v_d - v_s)^2 + 4v_r^2} - v_d - 2v_r - v_s\right),$$
$$\lambda_+ = \frac{1}{2}\left(\sqrt{(v_d - v_s)^2 + 4v_r^2} - v_d - 2v_r - v_s\right),$$

where obviously $\lambda_- < 0$ for any $v_r, v_d, v_s > 0$. Hence, $\lambda_+ < 0$ also remains to be shown. To this end, we start by assuming that $\lambda_+ > 0$; so we assume that

$$0 < \sqrt{u} - v,$$

with

$$u = (v_d - v_s)^2 + 4v_r^2$$

and

$$v = v_d + 2v_r + v_s.$$

We can safely multiply both sides of this inequality with something positive such as $\sqrt{u} + v$ and we therefore find that

$$\begin{aligned} 0 &< \left(\sqrt{u} - v\right)\left(\sqrt{u} + v\right) \\ &= u - v^2 \\ &= -4\left(v_d v_r + v_d v_s + v_r v_s\right) \end{aligned}$$

and, since $v_r, v_d, v_s > 0$, this is a contradiction and we conclude that $\lambda_+ < 0$ for all $v_r, v_d, v_s > 0$.

5.1.4 Properties of the Solution of the Stochastic Release Model

We have found that when the channel is closed, the equilibrium solution is given by

$$x_c = c_0,$$
$$y_c = c_1,$$

which is stable. Similarly, when the channel is open, the equilibrium solution is given by

$$x_o = \alpha c_1 + (1-\alpha)\, c_0, \text{ with } \alpha = \frac{v_r v_s}{v_d\,(v_r + v_s) + v_r v_s},$$
$$y_o = \beta c_1 + (1-\beta)\, c_0, \text{ with } \beta = \frac{v_s\,(v_d + v_r)}{v_d\,(v_r + v_s) + v_r v_s},$$

and this solution is also stable. The solution of the model given by the system (5.1) and (5.2) will therefore tend toward (x_c, y_c) whenever the channel is closed and toward (x_o, y_o) whenever the channel is open. This will be illustrated in numerical simulations below.

5.1.5 Numerical Scheme for the 2D Release Model

To perform 2D stochastic simulations, we use the numerical scheme

$$x_{n+1} = x_n + \Delta t\,(\gamma_n v_r\,(y_n - x_n) + v_d\,(c_0 - x_n)), \tag{5.11}$$
$$y_{n+1} = y_n + \Delta t\,(\gamma_n v_r\,(x_n - y_n) + v_s\,(c_1 - y_n)), \tag{5.12}$$

where γ is computed according to the Markov model given by the reaction scheme

$$C \underset{k_{co}}{\overset{k_{oc}}{\leftrightarrows}} O \tag{5.13}$$

(see page 28), where k_{oc} and k_{co} are reaction rates that may depend on both the concentrations represented by $x = x(t)$ and $y = y(t)$.

Table 5.1 Values of parameters used in 2D simulations based on the scheme (5.11) and (5.12)

v_d	1 ms^{-1}
v_r	0.1 ms^{-1}
v_s	0.01 ms^{-1}
c_0	0.1 μM
c_1	1,000 μM
k_{co}	1 ms^{-1}
k_{oc}	1 ms^{-1}

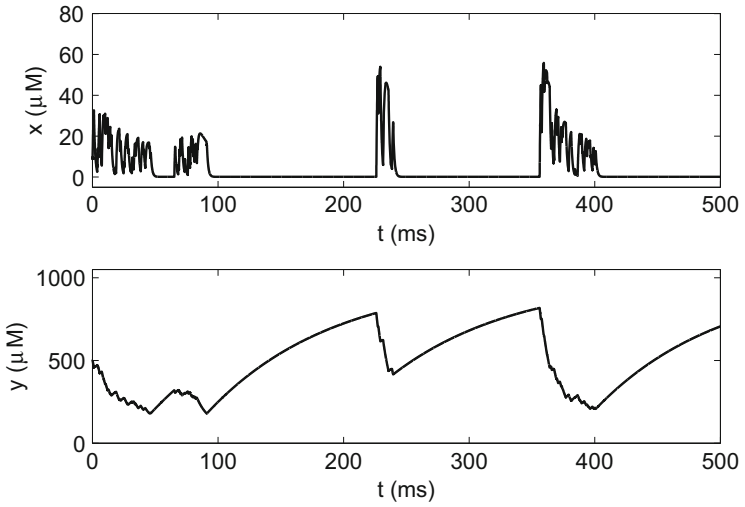

Fig. 5.3 Results of simulation using the scheme (5.11) and (5.12) with the data given in Table 5.1

5.1.5.1 Simulations Using the 2D Stochastic Model

We use the numerical scheme given by (5.11) and (5.12), where the parameters and functions involved are described in Table 5.1. The numerical solutions are given in Figs. 5.3 and 5.4. In the latter figure, we also indicate when the channel is open and closed (upper panel).

5.1.6 Invariant Region for the 2D Case

We observed in the 1D case that an invariant region for the numerical scheme used to compute approximate solutions of the stochastic model was useful for the probability density system, since it defined the interval in which to solve the system. Similarly, we will derive an invariant region for numerical solutions generated by the scheme (5.11) and (5.12) and this invariant region will define the geometry we will use to solve the probability density system.

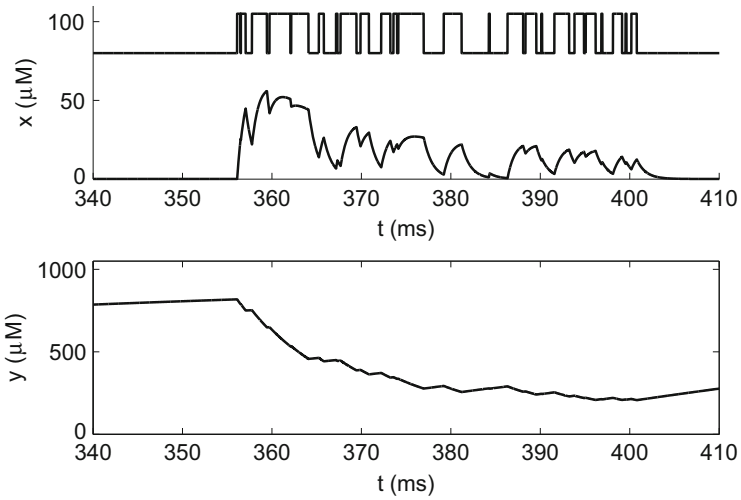

Fig. 5.4 A detailed view of the results given in Fig. 5.3. The open/closed state of the channel is indicated in the *upper panel*

Let us start by recalling the assumptions (5.3) and (5.4) and let us also assume that the time step $\Delta t > 0$ is chosen such that

$$\Delta t < \min\left(\frac{1}{v_r + v_d}, \frac{1}{v_r + v_s}\right). \tag{5.14}$$

Define

$$x_- = c_0, \tag{5.15}$$

$$x_+ = \frac{v_r c_1 + v_d c_0}{v_r + v_d}, \tag{5.16}$$

$$y_- = \frac{c_0 v_r + c_1 v_s}{v_r + v_s}, \tag{5.17}$$

$$y_+ = c_1, \tag{5.18}$$

and observe that

$$y_- - x_+ = \frac{c_0 v_r + c_1 v_s}{v_r + v_s} - \frac{v_r c_1 + v_d c_0}{v_r + v_d} = (c_1 - c_0)\,\frac{v_d v_s - v_r^2}{(v_r + v_s)\,(v_r + v_d)}.$$

It now follows from the assumptions (5.3) and (5.4) that we have

$$y_- \geqslant x_+. \tag{5.19}$$

Our aim is now to show that $\Omega = (x_-, x_+) \times (y_-, y_+)$ is an invariant region for solutions of the scheme (5.11) and (5.12). Because of (5.19), this means, in particular, that under the assumptions (5.3) and (5.4) the lowest possible calcium concentration of the JSR will always be larger than (or equal to) the highest calcium concentration of the dyad.

The numerical scheme (5.11, 5.12) can be written in the form

$$\begin{aligned} x_{n+1} &= F(x_n, y_n, \gamma_n), \\ y_{n+1} &= G(x_n, y_n, \gamma_n), \end{aligned}$$

where

$$\begin{aligned} F(x, y, \gamma) &= x + \Delta t \left(\gamma v_r (y - x) + v_d (c_0 - x)\right), \\ G(x, y, \gamma) &= y + \Delta t \left(\gamma v_r (x - y) + v_s (c_1 - y)\right). \end{aligned}$$

We will consider the properties of the functions F and G for x and y in the domain

$$\Omega = \{(x, y) : x_- \le x \le x_+,\ y_- \le y \le y_+\} \tag{5.20}$$

and for $0 \le \gamma \le 1$. Note that

$$\frac{\partial F(x, y, \gamma)}{\partial x} = 1 - \Delta t \left(\gamma v_r + v_d\right) \ge 1 - \Delta t \left(v_r + v_d\right) > 0$$

by condition (5.14). In addition, we have

$$\frac{\partial F(x, y, \gamma)}{\partial y} = \Delta t \gamma v_r \ge 0$$

and

$$\frac{\partial F(x, y, \gamma)}{\partial \gamma} = \Delta t v_r (y - x) \ge 0,$$

where we use (5.19) and (5.20). Similarly, we have

$$\frac{\partial G(x, y, \gamma)}{\partial y} = 1 - \Delta t \left(\gamma v_r + v_s\right) \ge 1 - \Delta t \left(v_r + v_s\right) > 0,$$

which is also positive by condition (5.14). Finally, we have

$$\frac{\partial G(x, y, \gamma)}{\partial x} = \Delta t \gamma v_r \ge 0$$

and

$$\frac{\partial G(x,y,\gamma)}{\partial \gamma} = \Delta t v_r (x-y) \leq 0$$

by (5.19) and (5.20). We now assume that

$$(x_n, y_n) \in \Omega .$$

Then,

$$x_{n+1} = F(x_n, y_n, \gamma_n) \geq F(x_-, y_-, 0) = x_-$$

and

$$x_{n+1} = F(x_n, y_n, \gamma_n) \leq F(x_+, y_+, 1) = x_+.$$

So we conclude that

$$x_- \leq x_{n+1} \leq x_+.$$

Similarly,

$$y_{n+1} = G(x_n, y_n, \gamma_n) \geq G(x_-, y_-, 1) = y_-$$

and

$$y_{n+1} = G(x_n, y_n, \gamma_n) \leq G(x_+, y_+, 0) = y_+;$$

so we conclude that

$$y_- \leq y_{n+1} \leq y_+.$$

We have seen that under the assumptions (5.3), (5.4), and (5.14), it follows that, if

$$(x_n, y_n) \in \Omega ,$$

then also

$$(x_{n+1}, y_{n+1}) \in \Omega$$

and we therefore conclude that Ω is an invariant region for the scheme of (5.11) and (5.12). This means that the probability density system will be solved in the domain defined by Ω.

5.2 Probability Density Functions in 2D

In the 1D case considered above, we derived a model for the probability density functions. In the 2D case, we can follow exactly the same steps and arrive at a system of partial differential equations of the form

$$\frac{\partial \rho_o}{\partial t} + \frac{\partial}{\partial x}\left(a_o^x \rho_o\right) + \frac{\partial}{\partial y}\left(a_o^y \rho_o\right) = k_{co}\rho_c - k_{oc}\rho_o, \tag{5.21}$$

$$\frac{\partial \rho_c}{\partial t} + \frac{\partial}{\partial x}\left(a_c^x \rho_c\right) + \frac{\partial}{\partial y}\left(a_c^y \rho_c\right) = k_{oc}\rho_o - k_{co}\rho_c, \tag{5.22}$$

where

$$\begin{aligned} a_o^x &= v_r\,(y - x) + v_d\,(c_0 - x)\,, \\ a_o^y &= v_r\,(x - y) + v_s\,(c_1 - y)\,, \\ a_c^x &= v_d\,(c_0 - x)\,, \\ a_c^y &= v_s\,(c_1 - y)\,. \end{aligned} \tag{5.23}$$

As in 1D, ρ_o and ρ_c denote the open and closed probability density functions, respectively, satisfying the integral condition

$$\int_\Omega (\rho_o + \rho_c)\,dx\,dy = 1. \tag{5.24}$$

Here the domain can be taken to be

$$\Omega = \{(x, y) : x_- \leqslant x \leqslant x_+,\ y_- \leqslant y \leqslant y_+\} \tag{5.25}$$

and the boundary conditions are again defined to ensure that there is no flux of probability out of the domain (see page 37).

5.2.1 Numerical Method for Computing the Probability Density Functions in 2D

To solve the system (5.21) and (5.22), we need to define a numerical method. For the 1D model (see page 37), we used an upwind scheme as presented by LeVeque [48]. Here, we use the 2D version of the same numerical method. Consider the partial differential equation

$$\rho_t + (a\rho)_x + (b\rho)_y = g\rho$$

Table 5.2 Discretization parameters

Δt	0.001 ms
Δx	0.92 μM
Δy	9.3 μM

where a, b, and g are smooth functions of x and y. We let $\rho_{i,j}^n$ denote an approximation of ρ at time $t = n\Delta t$ for $(x, y) \in [x_{i-1/2}, x_{i+1/2}) \times [y_{j-1/2}, y_{j+1/2})$, where $x_i = x_- + i\Delta x$, $y_j = y_+ + j\Delta y$, and

$$\Delta x = \frac{x_+ - x_-}{M_x}, \ \Delta y = \frac{y_+ - y_-}{M_y}.$$

Here M_x and M_y denote the number of grid points along the x and y axes, respectively. The numerical approximation is defined by the scheme

$$\begin{aligned}\rho_{i,j}^{n+1} = \rho_{i,j}^n &- \frac{\Delta t}{\Delta x}\left((a\rho)_{i+1/2,j}^n - (a\rho)_{i-1/2,j}^n\right) \\ &- \frac{\Delta t}{\Delta y}\left((b\rho)_{i,j+1/2}^n - (b\rho)_{i,j-1/2}^n\right) + \Delta t g_{i,j}\rho_{i,j}^n,\end{aligned} \tag{5.26}$$

where

$$(a\rho)_{i+1/2,j}^n = \max(a_{i+1/2,j}, 0)\rho_{i,j}^n + \min(a_{i+1/2,j}, 0)\rho_{i+1,j}^n, \tag{5.27}$$

$$(b\rho)_{i,j+1/2}^n = \max(b_{i,j+1/2}, 0)\rho_{i,j}^n + \min(b_{i,j+1/2}, 0)\rho_{i,j+1}^n. \tag{5.28}$$

In our simulations, this scheme is used for both equations (5.21) and (5.22) above, where the right-hand sides are given by $k_{co}\rho_c - k_{oc}\rho_o$ and $k_{oc}\rho_o - k_{co}\rho_c$, respectively.

As pointed out above, the probability densities integrates to one (see (5.24)), and the discrete version of this condition reads,

$$\Delta x \Delta y \sum_{i,j} \rho_{i,j} = 1, \tag{5.29}$$

where $\rho = \rho_o + \rho_c$. Note that the initial conditions must be chosen such that this condition holds. The discretization parameters used throughout this chapter are given in Table 5.2.

5.2.2 Rapid Decay to Steady State Solutions in 2D

We observed in 1D that the time-dependent probability density functions converge rapidly toward steady state solutions. This is illustrated in Fig. 2.7 on page 39. In Fig. 5.5, we show snapshots of the open probability density function at times 1, 2,

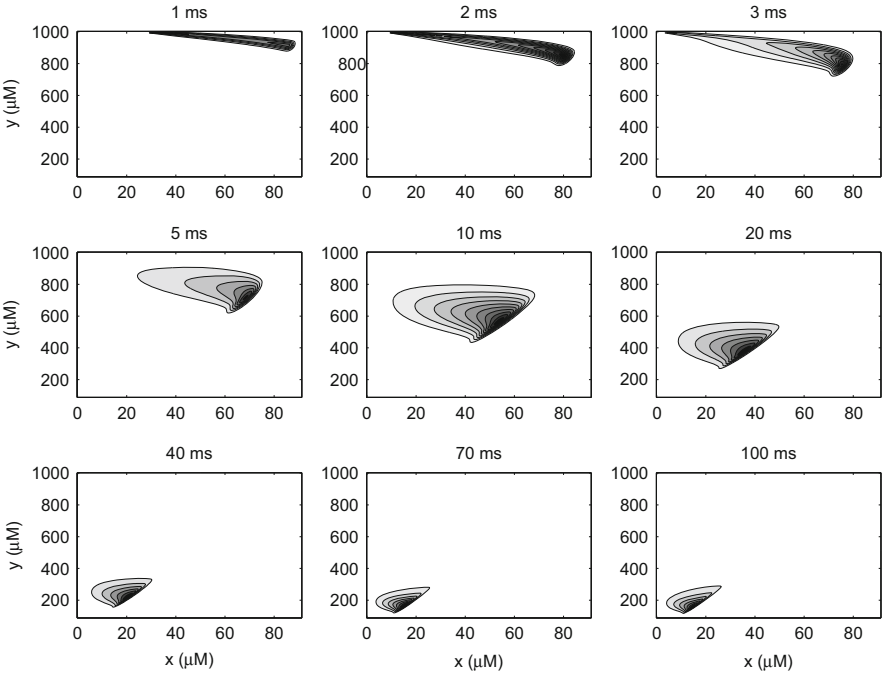

Fig. 5.5 Open probability density function ρ_o as a function of the dyad (x) and the JSR concentrations (y) for times $t = 1, 2, 3, 5, 10, 20, 40, 70$, and 100 ms. Note the convergence toward an equilibrium solution. In the computations, we use $\Delta t = 0.001$ ms, $\Delta x = 0.92$ μM, and $\Delta y = 9.3$ μM

3, 5, 10, 20, 40, 70, and 100 ms and we observe that the solution converges toward an equilibrium solution with time. This is verified in Fig. 5.6, where we plot the (weighted) norm between the dynamic and stationary solutions for time t ranging from 0 to 150 ms and we see that the solution is quite close to equilibrium at $t = 100$ ms. This observation is useful because it implies that when we assess the effect of various theoretical drugs, it is sufficient to consider steady state solutions.

5.2.3 *Comparison of Monte Carlo Simulations and Probability Density Functions in 2D*

As in 1D, we want to compare the probability densities ρ_o and ρ_c computed by solving the probability density system (5.21) and (5.22) using the scheme (5.26) with Monte Carlo simulations based on the stochastic differential equations (5.1) and (5.2) solved by the numerical scheme (5.11) and (5.12). The comparison is undertaken in the same manner as in 1D. We simply run a number of Monte Carlo

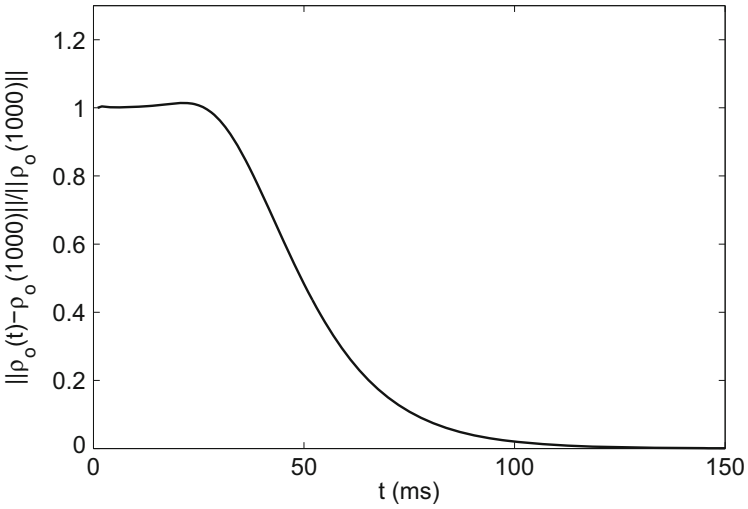

Fig. 5.6 The weighted norm of the difference between the open probability density function ρ_o at time t and at time 1,000 ms. This figure shows convergence toward an equilibrium solution

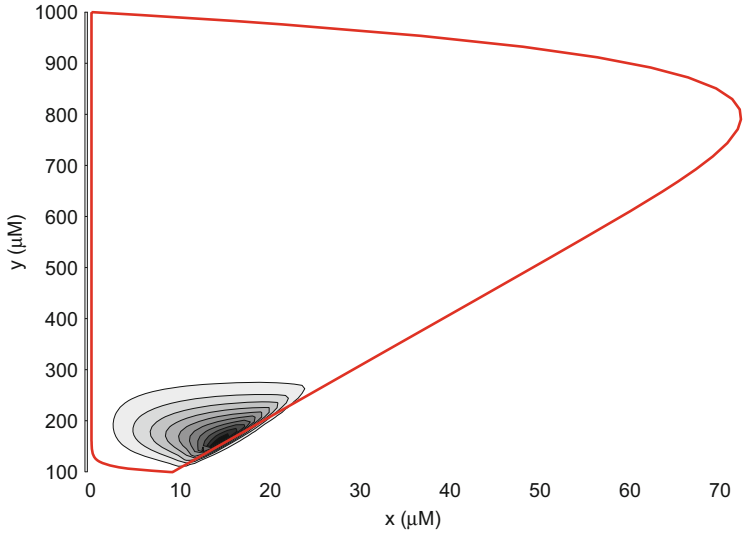

Fig. 5.7 Steady state open probability density function ρ_o computed by solving the probability density system (5.21) and (5.22). The solution is bounded (*red curve*) by solutions of the system (5.7) and (5.8) and the system (5.9) and (5.10)

simulations for a long time and count the number of open states in small rectangles. The procedure is a direct generalization of the method used in 1D (see page 40).

The numerical solution of the probability density system is given in Fig. 5.7 and the associated solution based on Monte Carlo simulations is given in Fig. 5.8. As in

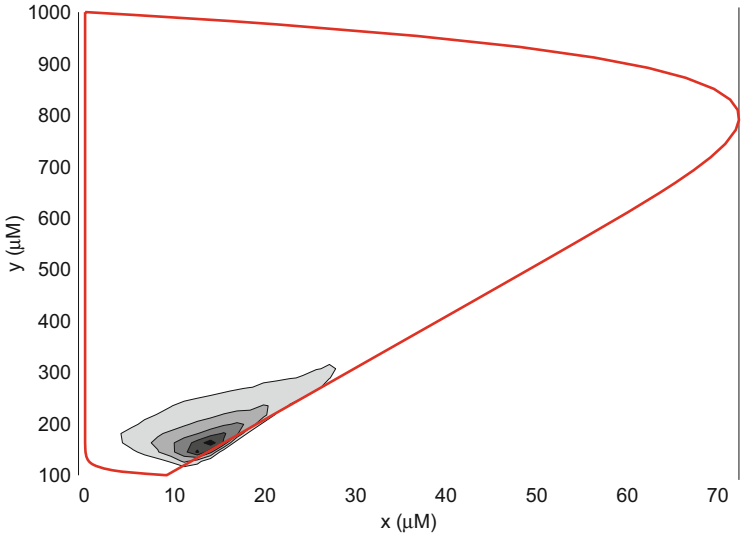

Fig. 5.8 Open probability density function ρ_o computed by Monte Carlo simulations using the scheme (5.11) and (5.12). The solution is bounded (*red curve*) by solutions of the system (5.7) and (5.8) and the system (5.9) and (5.10)

1D, we observe that the solutions are quite similar. In both these figures, we observe that the solutions stay inside a region bounded by a red curve. The red curve is computed by solving (5.7) and (5.8) for the closed state and (5.9) and (5.10) for the open state.

5.2.4 Increasing the Open to Closed Reaction Rate in 2D

In 1D, we observed that if we increased the reaction rate k_{oc} from open to closed, the steady state probability density functions changed considerably (see page 46). We observed that the open probability decreased and the closed probability increased significantly. In Fig. 5.9, we study the same effect in 2D and again we observe that the open probability density function is considerably decreased when k_{oc} is increased from one to three. The statistics of the solutions are given in Table 5.3 and we note that the total open probability is reduced considerably when k_{oc} is increased from one to three. The expected dyad concentration (x) does not change very much, but the expected JSR concentration (y) increases significantly and this observation holds for both open and closed channels.

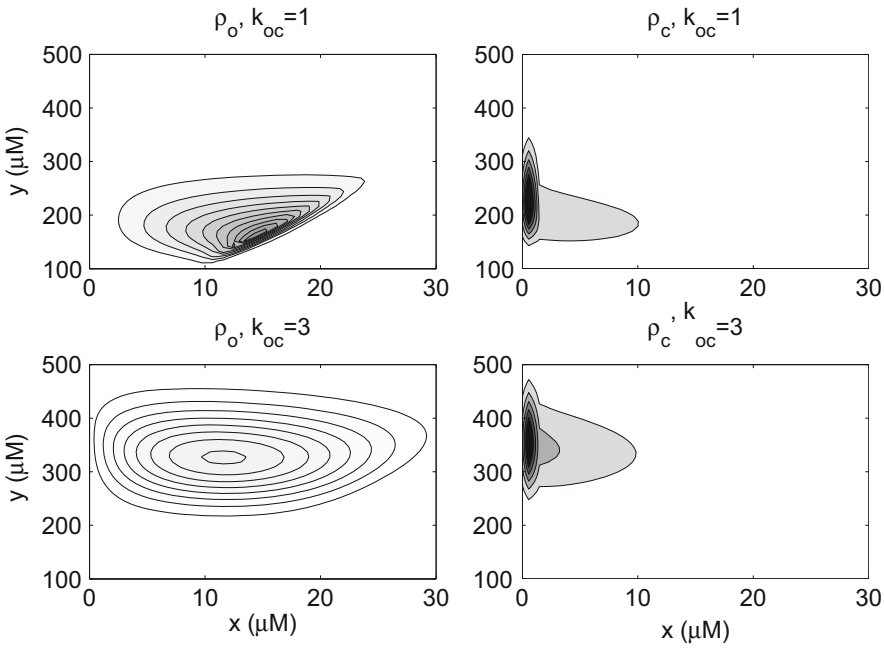

Fig. 5.9 The effect of increasing k_{oc} from one to three. The open probability density function is reduced considerably

Table 5.3 Statistical properties of the probability density functions for $k_{oc} = 1\ \text{ms}^{-1}$ and $k_{oc} = 3\ \text{ms}^{-1}$

k_{oc}	π_o	E_{x_o}	E_{y_o}	σ_{x_o}	σ_{y_o}
1	0.430	12.63	202.4	4.948	46.27
3	0.221	13.23	339.2	6.723	56.88
k_{oc}	π_c	E_{x_c}	E_{y_c}	σ_{x_c}	σ_{y_c}
1	0.570	5.12	218.2	4.842	49.90
3	0.779	5.95	348.0	5.563	57.22

5.3 Notes

1. The 2D stochastic model and the associated probability density functions are taken from Huertas and Smith [35], but some of the parameters are changed.